



Inter-decadal change in potential predictability of the East Asian summer monsoon

Jiao Li¹ · Ruiqiang Ding^{2,3} · Zhiwei Wu⁴ · Quanjia Zhong² · Baosheng Li² · Jianping Li^{5,6}

Received: 29 November 2017 / Accepted: 11 April 2018
© Springer-Verlag GmbH Austria, part of Springer Nature 2018

Abstract

The significant inter-decadal change in potential predictability of the East Asian summer monsoon (EASM) has been investigated using the signal-to-noise ratio method. The relatively low potential predictability appears from the early 1950s through the late 1970s and during the early 2000s, whereas the potential predictability is relatively high from the early 1980s through the late 1990s. The inter-decadal change in potential predictability of the EASM can be attributed mainly to variations in the external signal of the EASM. The latter is mostly caused by the El Niño–Southern Oscillation (ENSO) inter-decadal variability. As a major external signal of the EASM, the ENSO inter-decadal variability experiences phase transitions from negative to positive phases in the late 1970s, and to negative phases in the late 1990s. Additionally, ENSO is generally strong (weak) during a positive (negative) phase of the ENSO inter-decadal variability. The strong ENSO is expected to have a greater influence on the EASM, and vice versa. As a result, the potential predictability of the EASM tends to be high (low) during a positive (negative) phase of the ENSO inter-decadal variability. Furthermore, a suite of Pacific Pacemaker experiments suggests that the ENSO inter-decadal variability may be a key pacemaker of the inter-decadal change in potential predictability of the EASM.

1 Introduction

The East Asian summer monsoon (EASM) has become an indispensable part of the Asian summer monsoon system

✉ Ruiqiang Ding
drq@mail.iap.ac.cn

✉ Zhiwei Wu
zhiweiwu@fudan.edu.cn

¹ Nanjing University of Information Science and Technology, Nanjing 210044, Jiangsu, China

² State Key Laboratory of Numerical Modeling for Atmospheric Sciences and Geophysical Fluid Dynamics, Institute of Atmospheric Physics, Chinese Academy of Sciences, Beijing 100029, China

³ Plateau Atmosphere and Environment Key Laboratory of Sichuan Province, Chengdu University of Information Technology, Chengdu 610225, China

⁴ Institute of Atmospheric Sciences, Fudan University, Shanghai 200433, China

⁵ State Key Laboratory of Earth Surface Processes and Resource Ecology and College of Global Change and Earth System Science, Beijing Normal University, Beijing 100875, China

⁶ Laboratory for Regional Oceanography and Numerical Modeling, Qingdao National Laboratory for Marine Science and Technology, Qingdao 266237, China

(Ding 1992; Tao and Chen 1987; Zhao et al. 2016). The EASM shows complex spatiotemporal structures and is significantly influenced by the large thermal and orographic forcing between the largest ocean of the world, the Pacific, and the largest global continent, Eurasia. The EASM is also strongly affected by the highest land of the world, the Tibetan Plateau (Chen and Chang 1980; Wang et al. 2008b). Droughts and floods caused by variations of the EASM lead to large economic losses and influence the livelihoods of about one-third of the world's population (Huang et al. 2007). Consequently, the EASM has received much attention from researchers.

The nature of variations in the EASM during the twentieth century has been a subject of active research. Over the last decades, many research focus on the EASM on the decadal timescales. A large decadal regime shift appeared at the end of 1970s, which resulted in less rainfall over North China and South China, and floods over the middle-lower Yangtze River regions and western Japan (Nitta and Hu 1996; Xu 2001; Zhou et al. 2009). Concurrently, the associated large-scale monsoon circulation underwent abrupt decadal transitions (Kachi and Nitta 1997; Ding et al. 2008). In addition to this distinct climate regime shift, an abrupt decadal shift was also identified in the early 1990s with the rainfall over South China enhanced (Wu et al. 2010b). A southward transition in the rainfall structure began in the late 1970s, then entered a

transition period during 1979–1992, and finally stabilized during the mid-1990s (Liu et al. 2011). These decadal shifts caused extensive flooding and droughts, affecting human livelihoods and the economy of the EASM region.

There is considerable evidence that the EASM is closely associated with the El Niño–Southern Oscillation (ENSO). ENSO exerts a remote impact on the inter-decadal change of the EASM by modulating the location and intensity of the western North Pacific subtropical high (WNPSH) (Gong and Ho 2002; Wang et al. 2008c). Wang et al. (2000) proposed that the anomalous western North Pacific (WNP) anticyclone could be affected by the combinations of local SST cooling and the remote tropical central-eastern Pacific SST warming. Wang et al. (2008c) further linked the ENSO inter-decadal variation in the late 1970s with the overall coupling of the ENSO–EASM system.

In addition to the effect of ENSO on the inter-decadal change of the EASM, previous studies have found that this variability is closely associated with the Indian Ocean (IO) (Xue 2001; Ding et al. 2010). Specifically, Xue (2001) suggested that the ocean–atmosphere interactions in the IO and the WNP are important in the inter-decadal variation in the EASM. Ding et al. (2010) found that the significant correlation between the Indian Ocean Dipole and the EASM shows a phase transition in the late 1970s. In addition, other studies have reported that the inter-decadal EASM variability could be linked to the forcing over the Tibetan Plateau (Duan and Wu 2008), snow cover (Wang et al. 2008a; Ding et al. 2009), the Pacific decadal oscillation (Zhu 2003), and aerosol forcing (Menon et al. 2002).

The atmosphere is a system with forced dissipative nonlinear, and predictability is an inherent attribute of the atmosphere (Lorenz 1963; Li and Chou 1997). Atmospheric predictability relies on the atmosphere initial state (Lorenz 1965). The inter-decadal shift in the EASM is expected to be associated with an inter-decadal change in potential predictability of the EASM. The potential predictability of the South Asian summer monsoon has substantially reduced in recent decades, due mainly to a large decline in external forcing (Goswami 2004). However, the inter-decadal changes in potential predictability of the EASM remain unknown. Therefore, this study aims to examine the inter-decadal change in potential predictability of the EASM, and to explore the possible causes.

The structure of the paper is outlined as follows. The data and method are described in Section 2. Section 3 identifies the inter-decadal change in potential predictability of the EASM and explores the possible causes of these changes. Pacemaker experiments are used to verify the conclusions drawn in this

section. Finally, Section 4 presents discussions and conclusion.

2 Data and method

2.1 Data

2.1.1 Observations

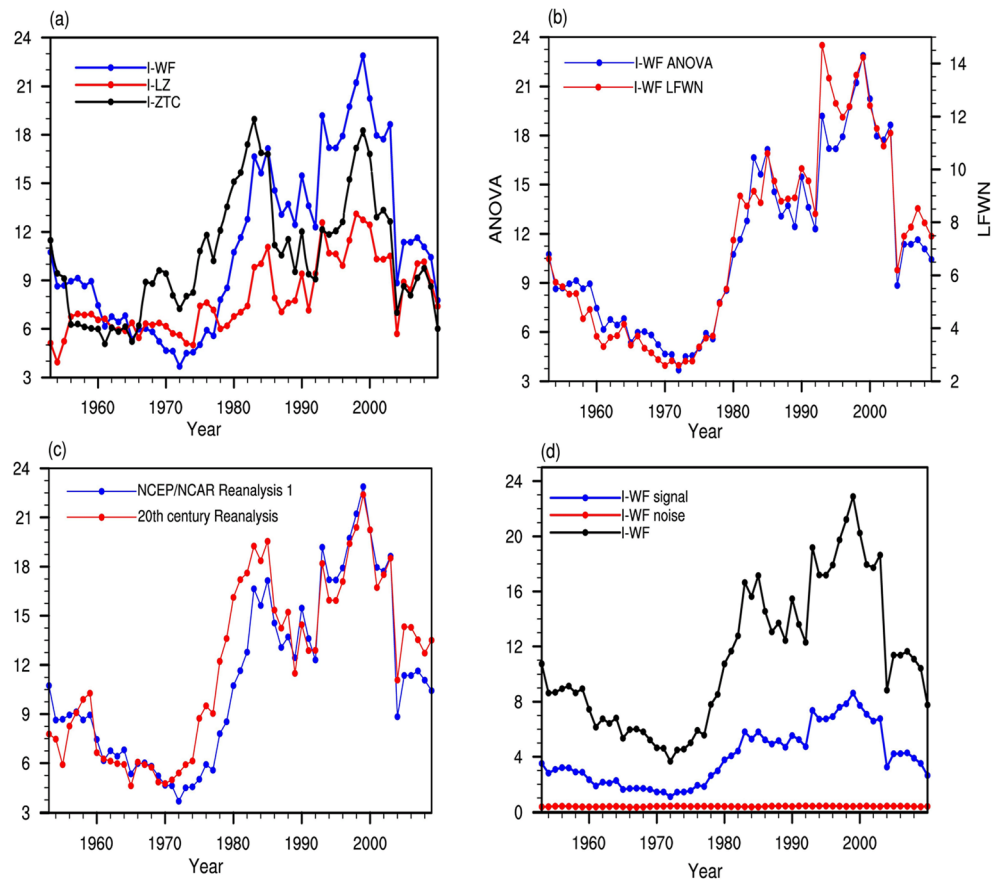
The monthly mean SST from the National Oceanic and Atmospheric Administration (NOAA) Extended Reconstructed SST version 3b (ERSSTv3b) with a resolution of 2° in longitude by 2° in latitude for the period 1854–2015 (Smith et al. 2008) is used here. The monthly (daily) mean atmospheric fields are taken from the National Centers for Environmental Prediction (NCEP1) reanalysis data with a horizontal resolution of $2.5^\circ \times 2.5^\circ$ during 1948–2015 (Kalnay et al. 1996). The 850 hPa geopotential height and wind datasets come from the NCEP/NCAR reanalysis. We also analyze the NOAA 20th Century Reanalysis version 2 (20CRv2) dataset with a horizontal resolution of $2^\circ \times 2^\circ$ to identify the results from the NCEP/NCAR reanalysis product (Compo et al. 2011). Three ENSO indices (Niño3, Niño4, and Niño3.4) come from the Climate Prediction Center (CPC; <http://www.cpc.noaa.gov>). The ENSO episodes come from the CPC (<http://www.cpc.ncep.noaa.gov>). In this study, the boreal summer is referred as June–August (JJA).

2.1.2 Monsoon indices

The EASM shows complex spatiotemporal structures (Tao and Chen 1987; Ding 1992). Precipitation patterns of the EASM show wide spatial variations that lead to difficulties in quantifying the EASM variability with rainfall. Thus, many studies have adopted circulation variables to measure the EASM; however, the representation of EASM circulation intensity remains debated. Five types of circulation indices exist regarding the complex structures of the EASM (Wang et al. 2008b): (1) the index that captures the East Asia and the WNP sea surface pressure difference (Guo 1983); (2) the index defined by zonal wind vertical shear (Webster and Yang 1992); (3) the vorticity shear index, which is the gradient between the north and south zonal winds (Huang and Yan 1999; Wang and Fan 1999; Zhang et al. 2003); (4) the southwesterly monsoon index, which uses the 850-hPa southwest wind to determine the intensity of the EASM (Li and Zeng 2002); and (5) the South China Sea monsoon index (Liang et al. 1999).

Wang et al. (2008b) used the multivariate empirical orthogonal function analysis method to evaluate 25 circulation indices by analyzing the circulation and precipitation systems of

Fig. 1 **a** Running mean SNR on an 11-year moving window for the period 1948–2015, using three EASM indices: I-WF (blue), I-LZ (red), and I-ZTC (black). **b** Running mean SNR (I-WF) on an 11-year moving window for the period 1948–2015, employing two methods: ANOVA (blue line, left y-axis) and LFWN (red line, right y-axis). **c** Running mean SNR (I-WF) on an 11-year moving window for the period 1948–2015 from two products: the NCEP/NCAR reanalysis1 product (blue) and the 20CRv2 product (red). **d** Running mean SNR using I-WF (black), signal variance using I-WF (blue), and noise variance using I-WF (red), for the period 1948–2015 (11-year moving window)



the EASM. The spatial pattern of the first mode was found to link accurately meridional dipole pattern with abundant rainfall over the Yangtze River, and suppressed precipitation over the Philippine Sea. While the spatial distribution of the second mode presented a diverse pattern, the principal components of the first mode leading were recommended to measure the EASM precipitation and circulation systems. These circulation indices, defined by Wang and Fan (1999) (hereafter I-WF), Zhang et al. (2003) (hereafter I-ZTC), and Li and Zeng (2002) (hereafter I-LZ) showed the relatively high correlations with the first leading principal component. All three indices were found to capture the westward extension of the WNPSH, weakened WNP monsoon trough, and strengthened southwesterly monsoon. In this study, we use these three indices to measure the EASM intensity.

2.2 Method

2.2.1 Signal-to-noise ratio method

The signal-to-noise ratio (SNR) method has been generally used to investigate atmospheric predictability (Trenberth

1985; Goswami 2004; Shi et al. 2008). The SNR estimates atmospheric predictability by quantifying the relative contributions of the predictable climate signal and the unpredictable climate noise. The climate signal is composed of contributions from slowly varying external forcing such as solar radiation, SST, sea ice, and various modes of the climate system, including ENSO, while the climate noise arises from internal dynamics, such as the intra-seasonal oscillation and daily weather fluctuations (Trenberth 1984). The SNR is quantified as the ratio (F) of the inter-annual variance of climate signal divided by the intra-seasonal variance of climate noise. The SNR is generally

Table 1 Correlation coefficients of SNR using three EASM indices

Correlation coefficient	SNR using I-WF	SNR using I-LZ	SNR using I-ZTC
SNR using I-WF	–	0.88*	0.72*
SNR using I-LZ	–	–	0.77*
SNR using I-ZTC	–	–	–

* All correlations are significant at or above the 5% significance level

Table 2 Correlation between the signal (noise) variance and the SNR of I-WF

Correlation coefficient	SNR using I-WF
Signal	0.99***
Noise	0.26

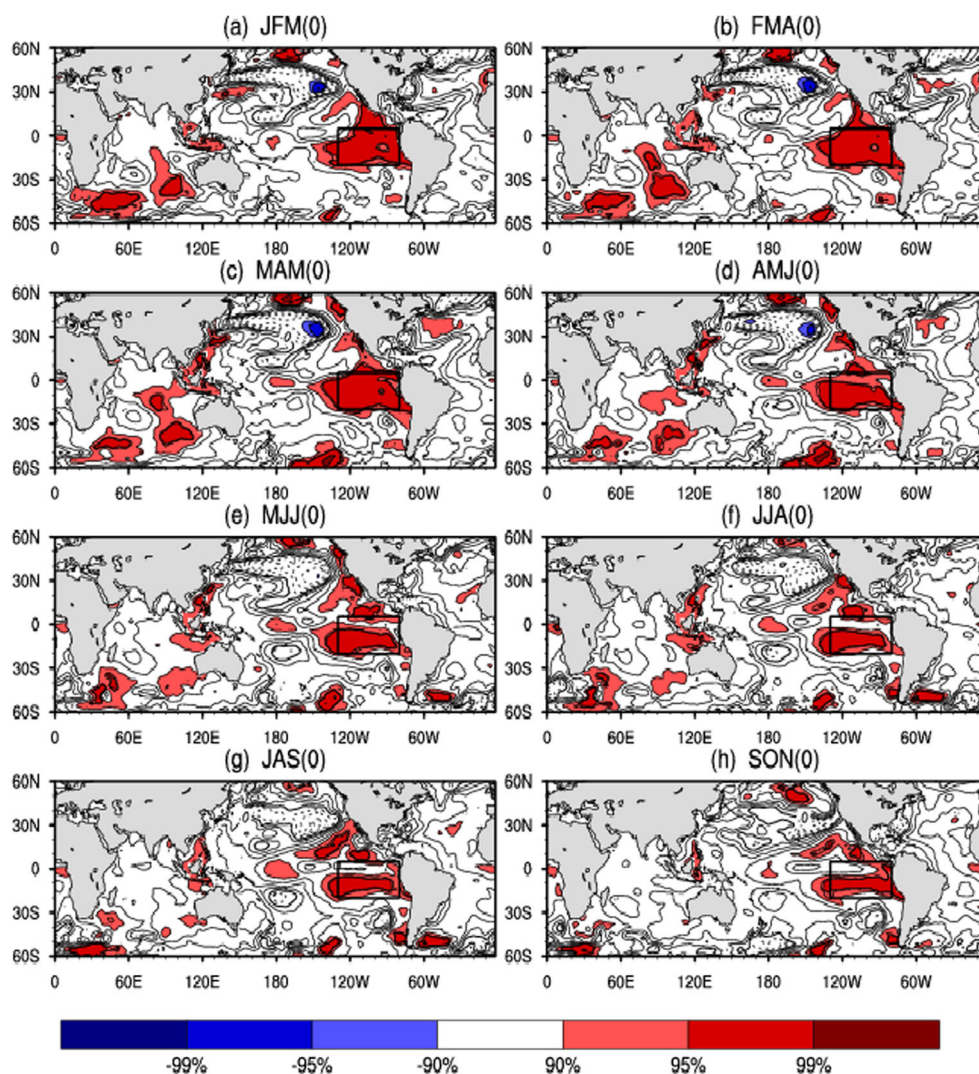
*** Correlation significant at the 99.9% level

computed by the following two methods: the low-frequency white noise extension (LFWN) (Madden 1976; Trenberth 1984) and the analysis of variance (ANOVA) (Jones 1975; Zheng et al. 2000). To examine the inter-decadal change in potential predictability of the EASM, the SNR method is applied to the three daily EASM indices (I-WF, I-LZ, and I-ZTC) based on an 11-year moving window in the study.

2.2.2 Pacemaker experiments

We use model output from a 10-member coupled model ensembles of the tropical Pacific Pacemaker simulations with the National Center for Atmospheric Research Community Earth System Model version 1.1.1 (NCAR CESM1.1.1). In the simulations, the spatial-temporal variations of the equatorial central-eastern Pacific SST anomalies (SSTAs) (15°S – 15°N , 180°W to the coast of South America) are nudged to observations (ERSSTv3b), and the rest of the modeled coupled climate system is free to evolve. All observational data used in the analysis are from the tropic central-eastern Pacific, which is strongly affected by ENSO. The model integrations start in 1920 and run through 2013, and the initial conditions of the ten ensemble members only differ.

Fig. 2 Correlation between the signal variance of I-WF and 3-month running averaged SSTAs (11-year moving window) for the period 1948–2015. The colored areas are the correlations significant at or above the 90% confidence level. The black rectangle indicates the region 5°N – 20°S , 130° – 80°W



To examine the relative impacts of external forcing variability (i.e., SST) and internal variability (i.e., daily weather fluctuations), the two components of the total variance of climate values are explored: the variance because of external forcing variability, and the variance due to internal variability. The latter is determined by studying model sensitivity to different initial atmospheric conditions. The potential predictability is measured as the absolute value of external forcing variance to the total variance (Rowell 1996; Rowell et al. 2010).

2.2.3 Effective number of degrees of freedom

Autocorrelations between two time series should be considered when estimating the significance of their correlation. The effective number of degrees of freedom will de-

crease due to the effect of autocorrelations. The effective sample size N^* is computed as follows (Bretherton et al. 1999; Ding et al. 2015):

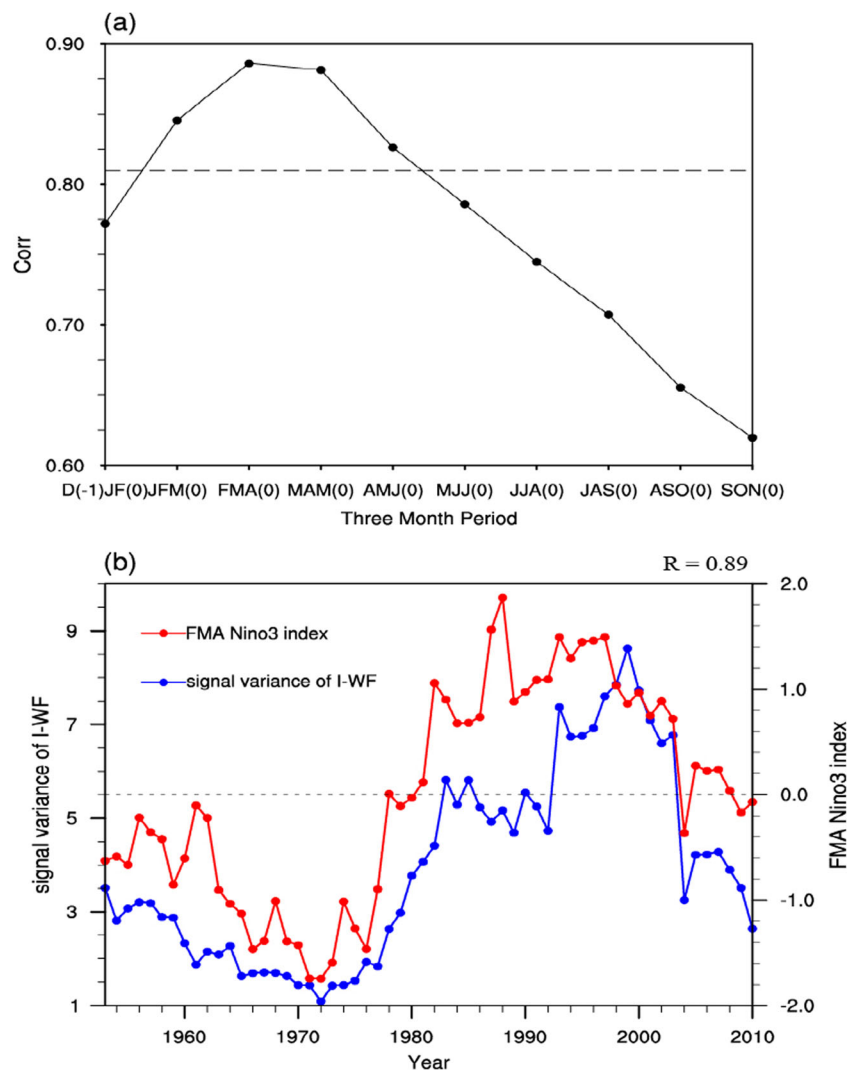
$$N^* = N \frac{1 - r_x r_y}{1 + r_x r_y}, \tag{1}$$

where N is the number of available time steps, and r_x and r_y are the lag-1 autocorrelations of variables x and y , respectively. Here, the method is employed to estimate the effective number of degrees of freedom.

3 Results

We first employ the ANOVA method to calculate the SNR of the three EASM indices: I-WF, I-LZ, and I-ZTC (Fig. 1a). The

Fig. 3 **a** Correlation coefficient between the signal variance of I-WF and the Niño3 index from D(-1)JF(0) to SON(0) on an 11-year moving window. The horizontal line represents the 95% confidence level. The “-1” denotes the previous year relative to year “0.” **b** The signal variance of I-WF (blue line, left y-axis) and the standardized FMA-averaged Niño3 index (red line, right y-axis) are calculated on an 11-year moving window for the period 1948–2015



SNR of I-WF shows a distinct inter-decadal variation from low to high values in the late 1970s, and a marked decline in the late 1990s. Similar results are gained from the SNR of I-LZ and I-ZTC, with correlation coefficients of the SNR of the three EASM indices varying between approximately 0.72 and 0.88 (Table 1). Furthermore, the SNR values of I-WF estimated by the LFWN and ANOVA method (Fig. 1b) are almost similar. The correlation of approximately 0.97 is significant at the 99.9% confidence interval, indicating that the SNR of the EASM is relatively independent of the SNR method used here. In addition, we compared the SNR of I-WF based on the NCEP1 and 20CRv2 products, and found that the SNR values of I-WF obtained from the two datasets are also similar ($r = 0.86$, significant at the 99.9% confidence interval; Fig. 1c). The results shown above imply that the SNR of the EASM is insensitive to the choice of dataset and method. Hereafter, we use I-WF and the ANOVA method to estimate the SNR of the EASM.

The above results show that the SNR of the EASM undergoes decadal shifts. To determine the cause of these variations, we examine the signal and noise variances of I-WF (Fig. 1d). Figure 1d shows that the signal variance resulting from external forcing undergoes an obvious decadal shift, concurrent with the SNR of I-WF ($r = 0.99$, significant at the 99.9% confidence interval; Table 2); however, the noise variance due to intra-seasonal activity and daily weather fluctuations does not undergo decadal transitions and remains low and constant for the whole period. These results further highlight that the inter-decadal change in SNR of the EASM is due mainly to variations in the external signal.

Previous studies found that slowly varying boundary conditions such as SST are an important external forcing of the variability in the EASM (Madden 1976; Shukla and Gutzler 1983; Trenberth 1984). Figure 2 displays the correlation between the external signal variance of I-WF and the 3-month averaged SSTAs from JFM(0) to SON(0). Hereafter, we denote the year of the SNR of the EASM as year (0) and the preceding year as year (-1). A remarkable positive correlation appears in the equatorial central-eastern Pacific during JFM(0), characterized by an ENSO-like pattern. The significant correlation increases from JFM(0), reaches a peak in FMA(0), and then persists through MJJ(0). The area-averaged SSTAs over the significant correlation area (5°N – 20°S , 130° – 80°W) of the tropical Pacific is correlated with the Niño3 index in FMA(0) with a correlation of about 0.95 that is significant at the 99% confidence interval. The correlation of the Niño3 index and the external signal variance of I-WF increases from D(-1)JF(0), and reaches a peak in FMA(0) (Fig. 3a). Hereafter, we employ FMA to replace FMA(0). Furthermore, the standardized FMA-averaged Niño3 index and the signal variance of I-WF are almost identical, with a

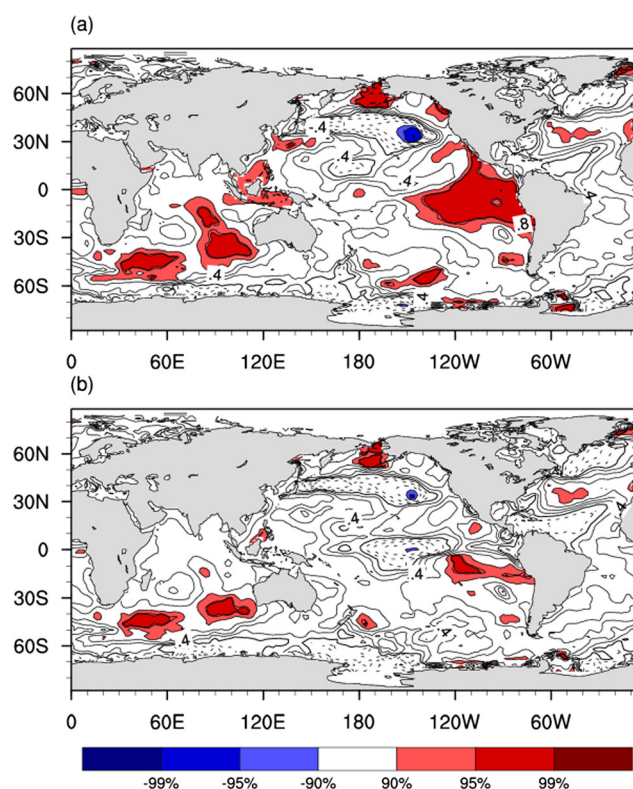


Fig. 4 Correlation maps of the signal variance of I-WF with **a** the FMA-averaged SSTAs and **b** the FMA-averaged SSTAs with the ENSO signal removed on an 11-year moving window for the period 1948–2015. The colored areas are the correlations significant at or above the 90% confidence level

correlation of approximately 0.89 (significant above the 95% confidence interval; Fig. 3b). Thus, the inter-decadal change in external signal/SNR of the EASM is mainly induced by variations in the phase of the ENSO inter-decadal variability, similar to previous study (Chan and Zhou 2005).

We also examine the partial correlation between the signal variance of I-WF and FMA-averaged SSTAs with the ENSO signal linearly removed (Fig. 4b). Figure 4b shows that the correlation is significantly reduced in the equatorial central-eastern Pacific during FMA compared to the correlation that the ENSO signal is not removed (Fig. 4a). This further confirms that the phase variations of the ENSO inter-decadal variability largely contribute to the inter-decadal external signal/SNR change of the EASM.

The external signal/SNR of the EASM primarily relies on the phase changes of the ENSO inter-decadal variability. The external signal/SNR of the EASM is high during a positive phase of the ENSO inter-decadal variability, and vice versa. Figure 5 shows that the frequency of El Niño events during a warm phase of the ENSO inter-decadal variability is higher than that during a cold phase.

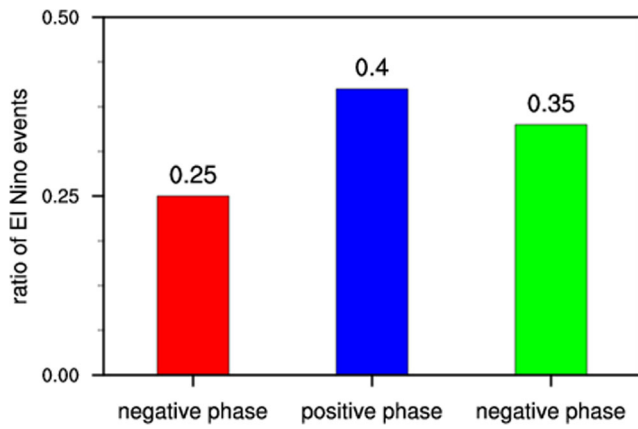


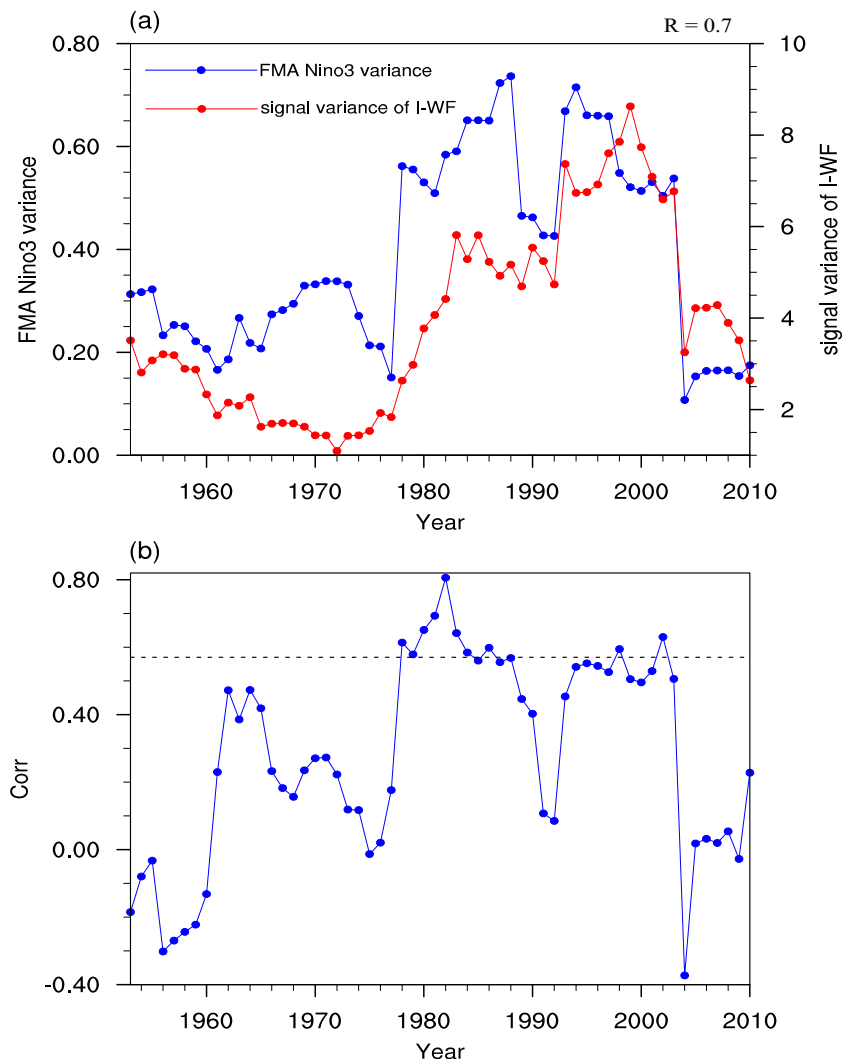
Fig. 5 The frequency of occurrence of El Niño events during the negative and positive phase of the ENSO inter-decadal variability

Therefore, the intensities of ENSO during a warm phase of the ENSO inter-decadal variability are usually stronger

than those in a cold phase of the ENSO inter-decadal variability. Strong ENSOs are expected to correlate with high external signals/SNRs of the EASM. To investigate this relationship, we compare the variance of the standardized FMA-averaged Niño3 index and the signal variance of I-WF (Fig. 6a). The two time series are similar, with a correlation of about 0.7 (significant at the 95% confidence interval). Our result suggests that the variations in the phase and intensity of the ENSO inter-decadal variability may lead to the inter-decadal changes in the external signal/SNR of the EASM. The strong ENSO generally corresponds to a high external signal/SNR of the EASM, and vice versa.

Next, we explore the inter-decadal change of relationship between the EASM and ENSO (Fig. 6b). Low correlations appear from the early 50s to the late 70s and during the early 2000s, while a high correlation occurs from the early 80s to

Fig. 6 **a** Variance of the standardized FMA-averaged Niño3 index (blue line; left y-axis) and the signal variance of I-WF (red line; right y-axis) calculated with an 11-year window for the period 1948–2015. **b** Sliding correlation between I-WF and the standardized FMA-averaged Niño3 index for the period 1948–2015 on an 11-year moving window. The horizontal line represents the 95% confidence level



the late 90s, as demonstrated by previous research (Wu et al. 2012c; Song and Zhou 2015). The sliding correlation indicates that ENSO is weakly correlated with the EASM during a cold phase of the ENSO inter-decadal variability, and relates to a strengthened relationship with the EASM during a warm phase of the ENSO inter-decadal variability.

The underlying physical processes by which ENSO modulates the EASM have drawn much attention (Wang et al. 2000; Yang et al. 2007; Wu et al. 2010a; Xie et al. 2016; Zhang et al. 2016). Wang et al. (2000) reported that ENSO exerts a great impact on the East Asian monsoon via the WNP anticyclone. Yang et al. (2007) argued that the IO warming induced by ENSO acts as a capacitor to drive the WNP anticyclone and affect the EASM. Xie et al. (2016) further explained that the IO warming could trigger a warm equatorial Kelvin wave that supports the WNP anticyclone.

Zhang et al. (2016) argued that the C-mode caused by the interactions between the annual cycle and the inter-annual variability of ENSO plays a main driver for modulating the EASM via the WNP anticyclone. These studies collectively posit that the ENSO has remote impacts on the East Asian monsoon via the WNP anticyclone. Thus, we further examine the changes in the WNP anticyclone during the periods with a low external signal (1953–1979, LE1; 2000–2010, LE2) and a high external signal (1980–1999, HE).

Figure 7a–o exhibits the regression of the 3-month averaged 850 hPa wind and geopotential height anomalies onto the FMA-averaged Niño3 index during the periods LE1, HE, and LE2. The regression spatial structures show obvious differences between the HE and LE1 (LE2) periods. During HE, an anomalous anti-cyclonic circulation

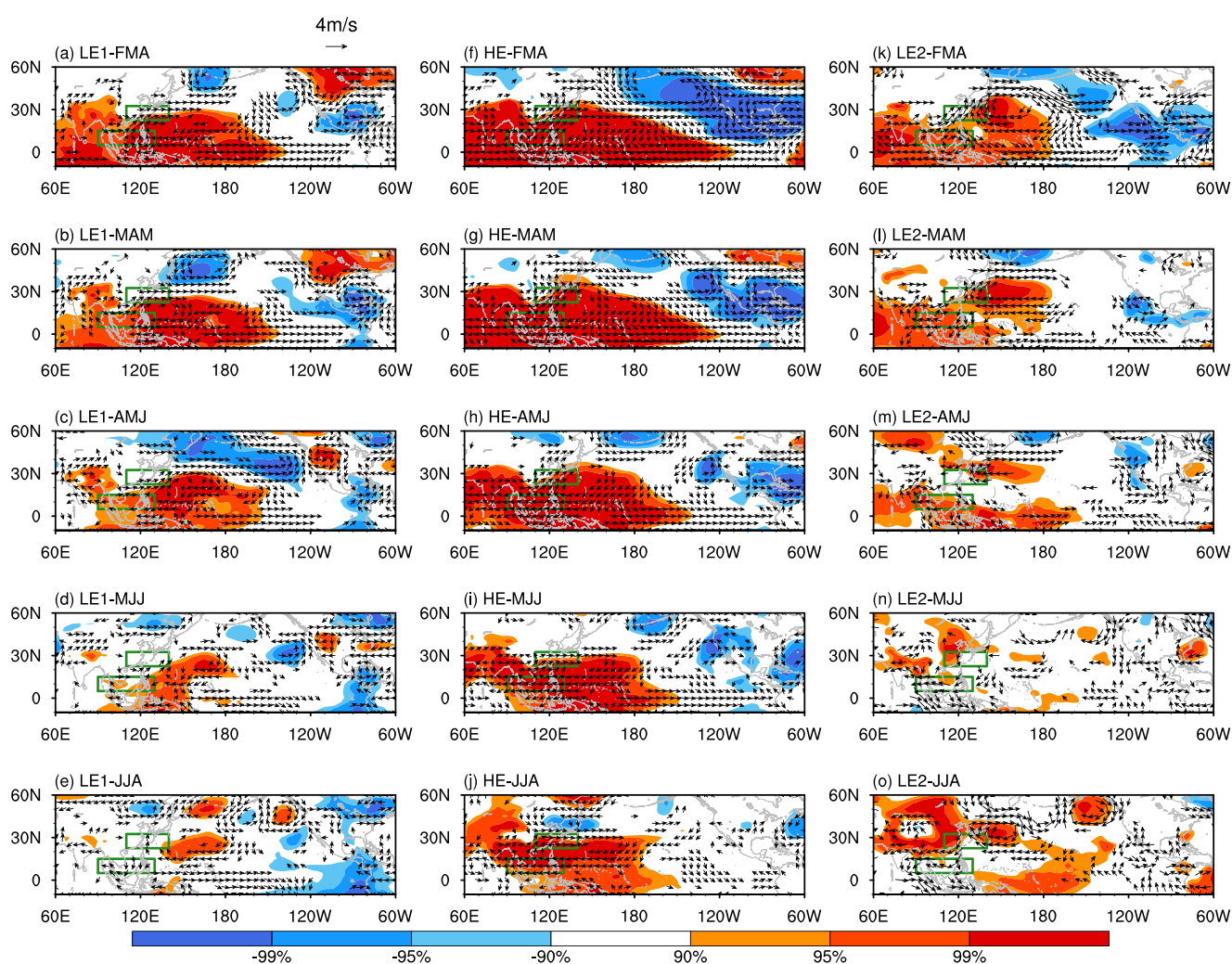


Fig. 7 Regressions of 3-month running 850-hPa wind and geopotential height anomalies onto the Niño3 index (FMA) for the **a–e** LE1, **f–j** HE, and **k–o** LE2 periods. The colored areas are significant at or above the

90% confidence level. The wind vectors are significant at the 90% confidence level. The green rectangles represent the two regions (90° – 130° E, 5° – 15° N; 110° – 140° E, 22.5° – 32.5° N) of I-WF

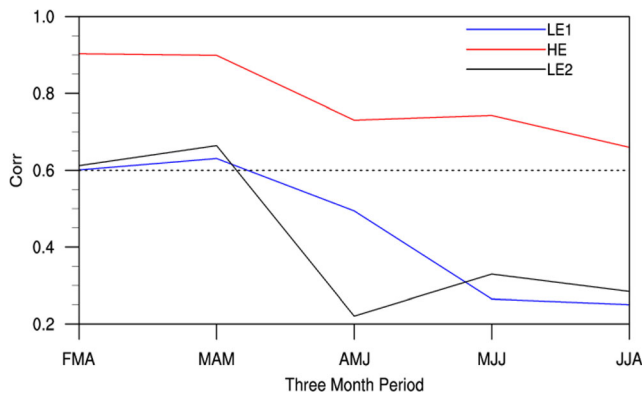


Fig. 8 Correlation coefficient between the WNP index and the Niño3 index from FMA to JJA for the LE1 (blue), HE (red), and LE2 (black) periods. The horizontal line represents the 95% confidence level

in FMA occupies the tropical western Pacific. The WNP anticyclone persists from FMA to JJA, affecting the concurrent EASM. In contrast, during both LE1 and LE2 the anticyclone in the tropical western Pacific is relatively weak from FMA to AMJ and vanishes in JJA. Thus, the southwesterly anomalies located at the edge of the WNP

anticyclone do not affect the simultaneous EASM. To further compare the WNP anticyclone between the LE1 and LE2, and HE periods, the WNP index is adopted (Sui et al. 2007) in Fig. 8 to quantify the intensity of the WNP anticyclone. The correlation between the FMA-averaged Niño3 index and the WNP index during the HE period is far higher (significant at the 95% confidence interval) than that during the LE1 and LE2 periods from FMA to JJA. Results indicate that ENSO induces a stronger effect on the EASM via the WNP anticyclone during the HE period. To better distinguish the influence on the EASM induced by ENSO between the LE1 and LE2, and HE periods, we compare the 3-month averaged 850-hPa moisture flux divergence anomalies and precipitation anomalies regressed onto the FMA-averaged Niño3 index for LE1 and LE2, and HE, respectively (Figs. 9 and 10). The regression patterns indicate distinct differences between the HE and LE1 (LE2) periods. During HE, the moisture flux divergence from FMA to JJA exhibits a pronounced dipole pattern with anomalous convergence along the Yangtze River, and anomalous divergence over the tropical western Pacific. By contrast, during LE1 and

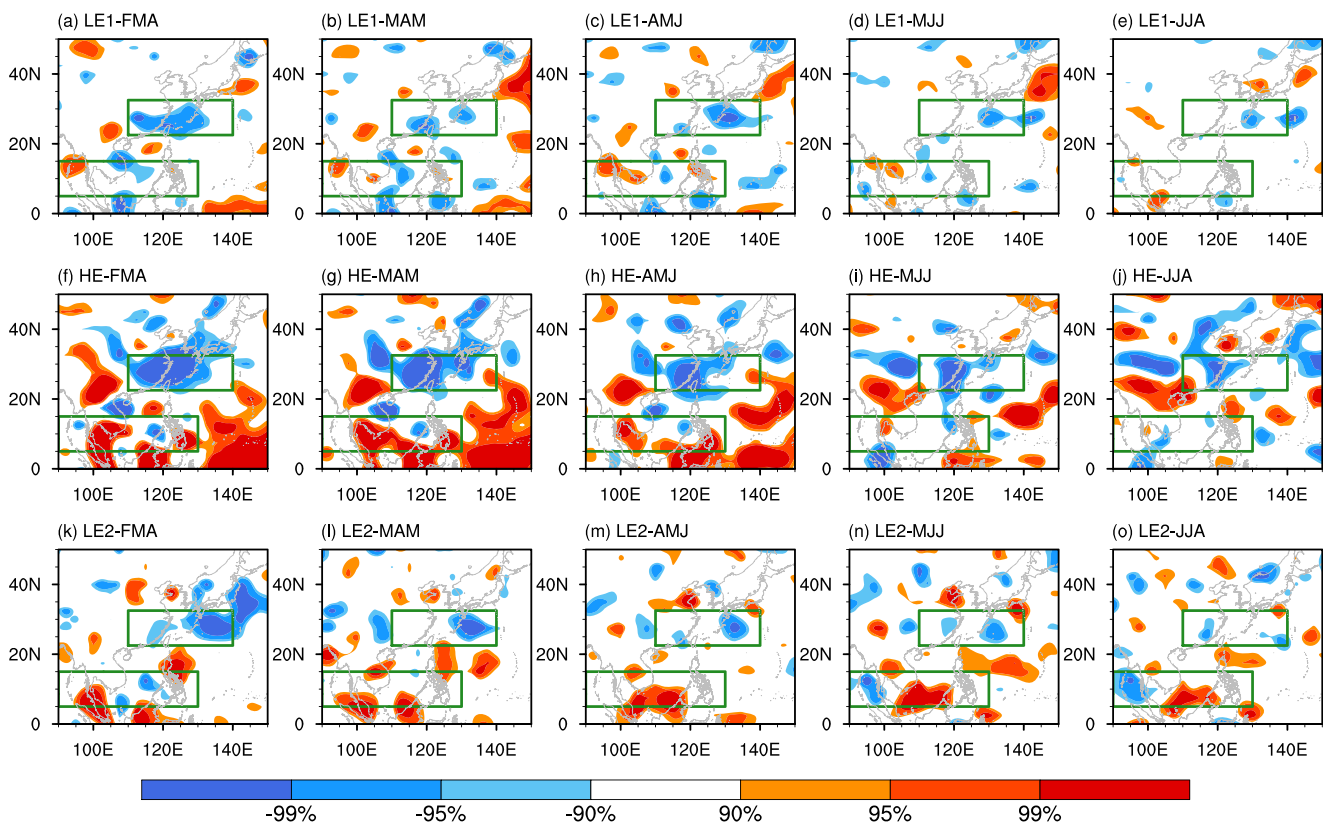


Fig. 9 Regressions of 3-month running 850-hPa moisture flux divergence anomalies onto the Niño3 index (FMA) for the a–e LE1, f–j HE, and k–o LE2 periods. The colored areas are significant at or above the

90% confidence level. The green rectangles represent the two regions (90°–130° E, 5°–15° N; 110°–140° E, 22.5°–32.5° N) of I-WF

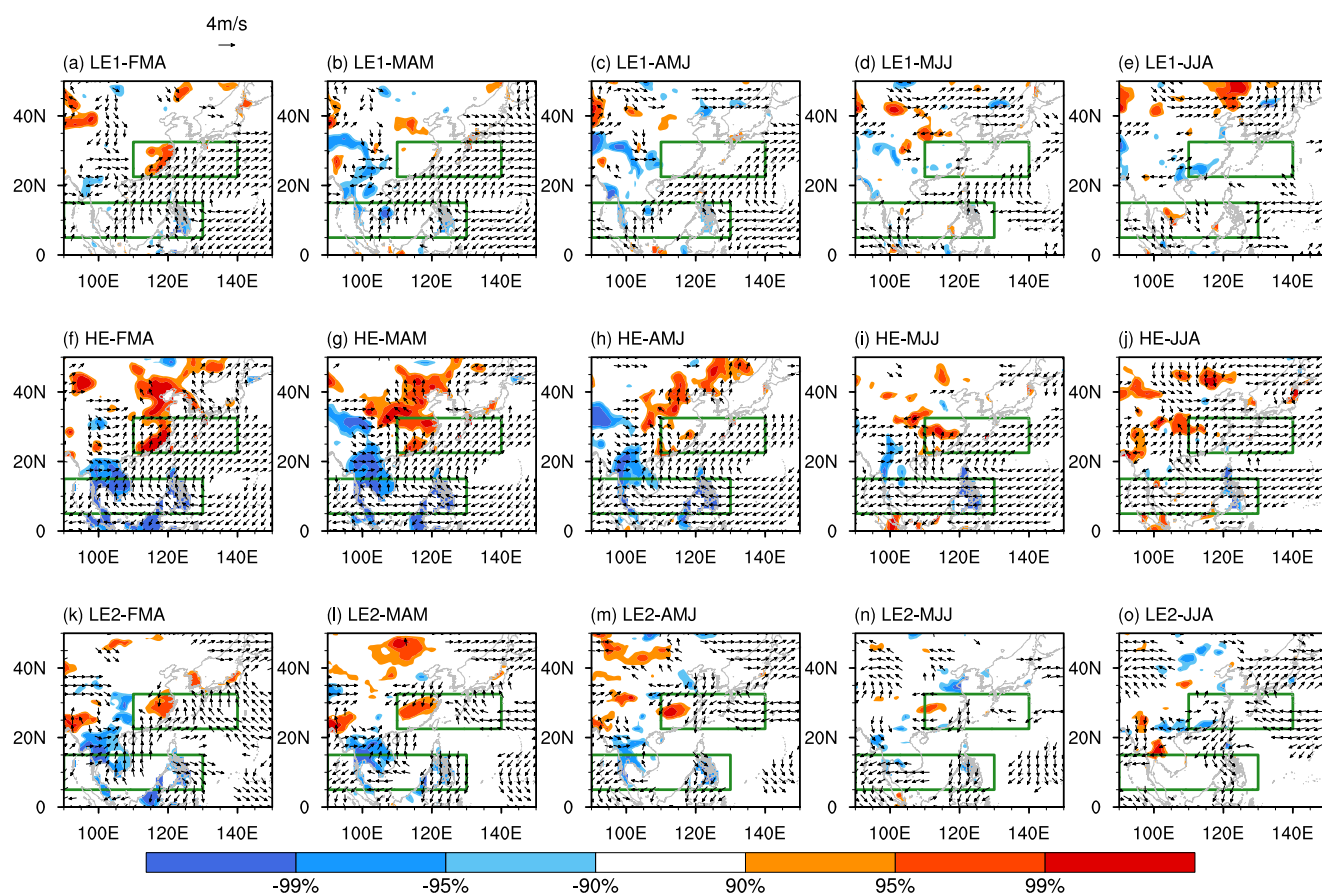


Fig. 10 Three-month running precipitation anomalies regressed onto the Niño3 index (FMA) for the **a–e** LE1, **f–j** HE, and **k–o** LE2 periods. The colored areas are significant at or above the 90% confidence level. The

wind vectors are significant at the 90% confidence level. The green rectangles represent the two regions (90°–130° E, 5°–15° N; 110°–140° E, 22.5°–32.5° N) of I-WF

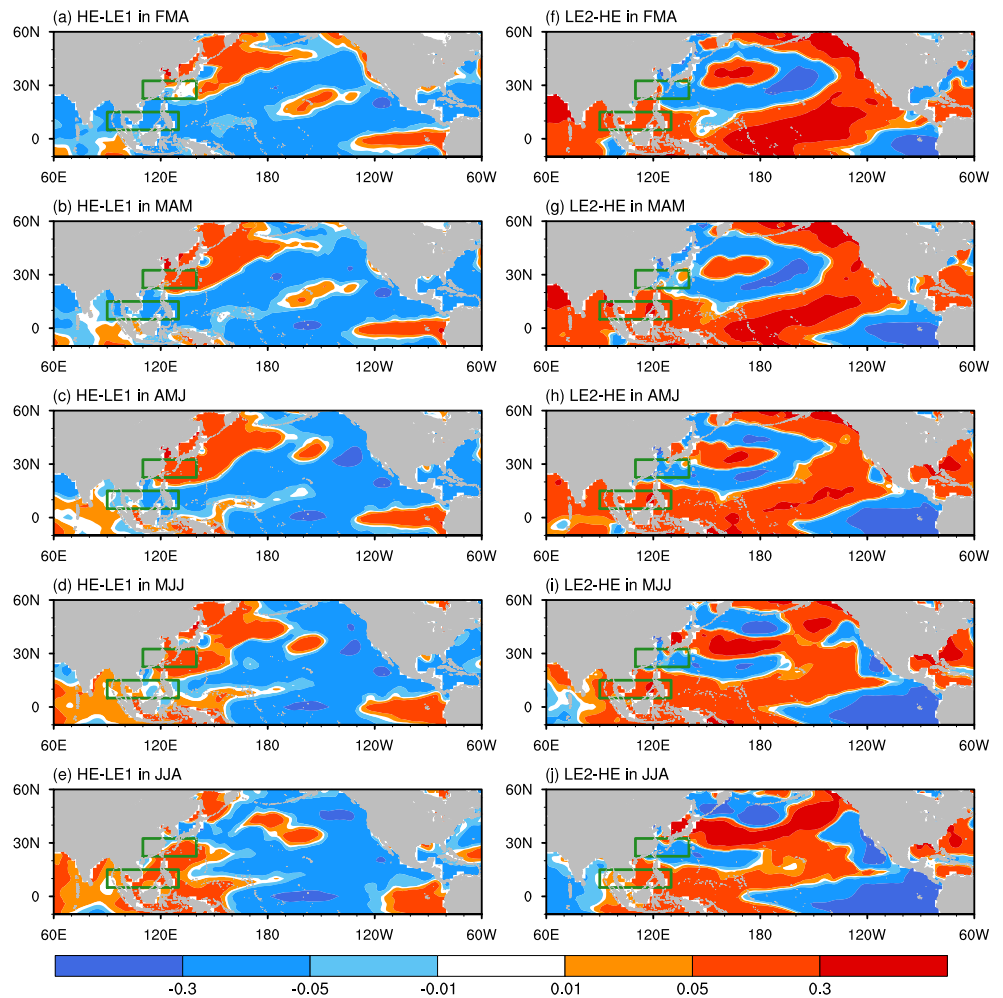
LE2, the dipole regression pattern does not exist from FMA to JJA (Fig. 9). Similarly, a noticeable north–south dipole precipitation regression pattern is found in the EASM region from FMA to JJA during the HE period; however, the dipole precipitation pattern is not observed during the LE1 and LE2 periods (Fig. 10). The above results suggest that ENSO could take a greater effect on the EASM in the HE period than in the LE1 and LE2 periods.

Next, we examine whether the changes in the phase and intensity of the ENSO inter-decadal variability could explain the inter-decadal variations in the external signal/SNR of the EASM. We investigate the difference in the regressions of the FMA-averaged Niño3 index onto 3-month averaged SSTs for the three periods (Fig. 11). Figure 11a–e displays the difference of the SSTA regressions during the HE and LE1 periods. The tropical central and eastern Pacific is characterized by positive SSTA regression anomalies from FMA to JJA. Figure 11f–j presents the difference in the SSTA regressions between the

LE2 and HE periods. Negative SSTA regression anomalies from FMA to JJA occur over the tropical central-eastern Pacific. Our results indicate that the tropical warm eastern Pacific SSTs during the HE period are greater than the tropical eastern Pacific SSTs during the LE1 and LE2 periods.

The decadal shifts in potential predictability of the EASM related to ENSO are reasonably well reproduced in the Pacific Pacemaker experiments from CESM. It should be noted that SST is allowed to interact with the atmospheric model, thus avoiding issues that are inherent to only atmosphere or ocean simulations (Cash et al. 2010). The potential predictability is computed as the absolute value of external forcing variance divided by total variance (Shi et al. 2008). The simulated potential predictability of the EASM shows distinct shifts, with low potential predictability during the LE1 and LE2 periods, and high potential predictability during the HE period, which is consistent with observations (Fig. 12). Therefore, in both simulations and observations, the inter-decadal

Fig. 11 Difference in the regressions of 3-month running SSTAs on the Niño3 index (FMA) between **a–e** the HE and LE1 periods, and **f–j** the LE2 and HE periods. The green rectangles represent the two regions (90°–130° E, 5°–15° N; 110°–140° E, 22.5°–32.5° N) of I-WF



variations in potential predictability of the EASM can be explained by the ENSO inter-decadal variability.

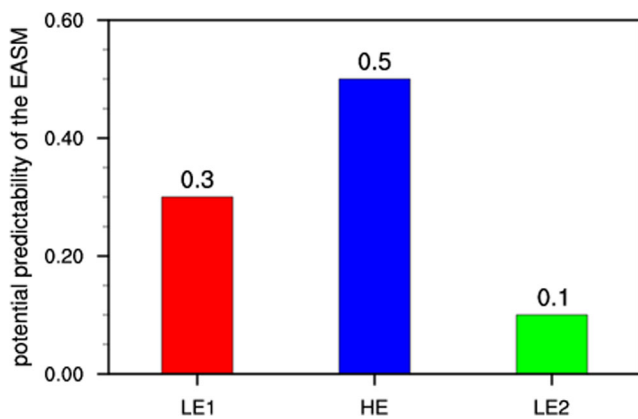


Fig. 12 The potential predictability of the EASM from pacemaker experiments for the LE1 (red), HE (blue), and LE2 (green) periods

4 Conclusions

The study explores the inter-decadal change in potential predictability of the EASM using the SNR method. The potential predictability of the EASM underwent a significant decadal change from a low to high phase at the end of 1970s, followed by a sharp decline at the end of 1990s. The inter-decadal change in potential predictability of the EASM is mainly generated by variations in the external signal of the EASM. The latter is attributable, at least in large part, to variations in the phase and intensity of the ENSO inter-decadal variability. As a major external signal of the EASM, the ENSO inter-decadal variability shifts to warm phases in the late 1970s, and then shifts to cold phases in the late 1990s. The frequency of occurrence of El Niño events during warm phases of the ENSO-like inter-decadal variability is found to be higher than that during cold phases. The ENSO intensity is usually stronger (weaker) during a positive (negative) phase of the ENSO inter-decadal variability.

Further analysis shows that a stronger ENSO has a more strengthened influence on the WNP anticyclone and hence the EASM, and vice versa. As a result, external forcing of the EASM from ENSO is enhanced during a warm phase of the ENSO inter-decadal variability, but weakens during a cold phase of the ENSO inter-decadal variability. The underlying mechanisms of these phenomena were investigated using a suite of Pacific Pacemaker experiments that indicate the observed inter-decadal change in potential predictability of the EASM is forced primarily by the ENSO inter-decadal variability.

Many previous studies have sought to enhance the prediction skills of the EASM, by using ideal simulations with the numerical model and statistical methods (Gadgil et al. 2005; Wu et al. 2009b; Wu and Yu 2016). Despite the efforts, the prediction skill of the EASM remains low. The present study shows that the potential predictability of the EASM has decreased since the late 1990s, which is unfavorable to improve the EASM predictions. The status of the EASM prediction skill in recent years may be due to the low potential predictability of the EASM. Ultimately, the findings in the paper would provide alternative physical explanation for the EASM prediction. Briefly, the interdecadal change in potential predictability of the EASM mainly depends on ENSO decadal variability. Thus, the EASM prediction on the basis of ENSO decadal variability is essential in practical forecast. The phase and intensity of the ENSO decadal variability could provide a reliable precursor for the EASM prediction.

In addition, the EASM is not only influenced by the tropical external forcing, such as ENSO, but also by middle and high latitude external forcing, such as Arctic sea ice (Wu et al. 2009a), forcing over the Tibetan Plateau (Wu et al. 2012a, b). Changes in external forcing over middle and high latitudes are expected to have effects on the inter-decadal trends in potential predictability of the EASM. Further analysis is required to investigate other possible causes of the potential predictability of the EASM on the decadal timescales. Furthermore, the intensity of the EASM in this study is measured using three EASM indices (Wang and Fan 1999; Li and Zeng 2002; Zhang et al. 2003) that capture the main components of the EASM circulation system. However, there still exist many other EASM indices that could describe the EASM system from other aspects. The inter-decadal change in potential predictability of the EASM may depend on the choice of EASM index. Therefore, further exploration of variations in potential predictability of the EASM, based on other EASM indices, is warranted.

Acknowledgments We acknowledge the helpful suggestions from the anonymous reviewers. We thank NCAR CESM for providing the Pacemaker experiment data (<http://www.cesm.ucar.edu/experiments/>). The reanalysis data including atmospheric fields was available at <https://www.esrl.noaa.gov/psd/data/gridded/>. The ENSO episodes come from the Climate Prediction Center (<http://www.cpc.ncep.noaa.gov>). We

also thank the ERSSTv3b data that is obtained from <https://www.esrl.noaa.gov/psd/data/gridded/data.noaa.ersst.v3.html>.

Author contribution This work is jointly supported by the National Natural Science Foundation of China for Excellent Young Scholars (41522502), the National Program on Global Change and Air-Sea Interaction (GASI-IPOVAI-03; GASI-IPOVAI-06), and the National Key Technology Research and Development Program of the Ministry of Science and Technology of China (2015BAC03B07).

References

- Bretherton CS, Widmann M, Dymnikov VP, Wallace JM, Bladé I (1999) The effective number of spatial degrees of freedom of a time-varying field. *J Clim* 12:1990–2009
- Cash BA, Rodó X, Kinter JL III, Yunus M (2010) Disentangling the impact of ENSO and Indian Ocean variability on the regional climate of Bangladesh: implications for cholera risk. *J Clim* 23:2817–2831
- Chan JCL, Zhou W (2005) PDO, ENSO and the early summer monsoon rainfall over south China. *Geophys Res Lett* 32:93–114
- Chen T-JG, Chang C-P (1980) The structure and vorticity budget of an early summer monsoon trough (Mei-Yu) over southeastern China and Japan. *Mon Weather Rev* 108:942–953
- Compo GP, Whitaker JS, Sardeshmukh PD, Matsui N, Allan RJ, Yin X, Gleason BE, Vose RS, Rutledge G, Bessemoulin P (2011) The twentieth century reanalysis project. *Q J Roy Meteor Soc* 137:1–28
- Ding R, Ha KJ, Li J (2010) Inter-decadal shift in the relationship between the East Asian summer monsoon and the tropical Indian Ocean. *Clim Dynam* 34:1059–1071
- Ding R, Li J, Tseng YH, Sun C, Guo Y (2015) The Victoria mode in the North Pacific linking extratropical sea level pressure variations to ENSO. *J Geophys Res* 120:27–45
- Ding Y (1992) Summer monsoon rainfalls in China. *J Meteorol Soc Jpn* 70:373–396
- Ding Y, Sun Y, Wang Z, Zhu Y, Song Y (2009) Inter-decadal variation of the summer precipitation in China and its association with decreasing Asian summer monsoon part II: possible causes. *Int J Climatol* 29:1926–1944
- Ding Y, Wang Z, Sun Y (2008) Inter-decadal variation of the summer precipitation in East China and its association with decreasing Asian summer monsoon. Part I: observed evidences. *Int J Climatol* 28:1139–1161
- Duan A, Wu G (2008) Weakening trend in the atmospheric heat source over the Tibetan Plateau during recent decades. Part I: observations. *J Clim* 21:3149–3164
- Gadgil S, Rajeevan M, Nanjundiah R (2005) Monsoon prediction—why yet another failure. *Curr Sci* 88:1389–1400
- Gong DY, Ho CH (2002) Shift in the summer rainfall over the Yangtze River valley in the late 1970s. *Geophys Res Lett* 29(10):78-1–78-4. <https://doi.org/10.1029/2001GL014523>
- Goswami B (2004) Inter-decadal change in potential predictability of the Indian summer monsoon. *Geophys Res Lett* 31(16):371–375
- Guo QY (1983) The summer monsoon intensity index in East Asia and its variation. *Acta Geograph Sin* 38:207–217
- Huang G, Yan Z (1999) The East Asian summer monsoon circulation anomaly index and its interannual variations. *Chin Sci Bull* 44:1325–1329
- Huang R, Chen J, Huang G (2007) Characteristics and variations of the East Asian monsoon system and its impacts on climate disasters in China. *Adv Atmos Sci* 24:993–1023
- Huang R, Liang Y, Song L (1992) Variability of summer droughts and floods in China during recent 40 years and primary investigation of its causes. LASG special research Collections: 14–28

- Jones RH (1975) Estimating the variance of time averages. *J Appl Meteorol* 14:159–163
- Ju JH, Qian C, Cao J (2005) The intraseasonal oscillation of East Asian summer monsoon. *Chin J Atmos Sci* 29:187–194
- Kachi M, Nitta T (1997) Decadal variations of the global atmosphere-ocean system. *J Meteorol Soc Jpn* 75:657–675
- Kalnay E, Kanamitsu M, Kistler R, Collins W, Deaven D, Gandin L, Iredell M, Saha S, White G, Woollen J (1996) The NCEP/NCAR 40-year reanalysis project. *B Am Meteorol Soc* 77:437–471
- Li J, Chou J (1997) Existence of the atmosphere attractor. *Sci China Ser D* 40:215–220
- Li J, Zeng Q (2002) A unified monsoon index. *Geophys Res Lett* 29:115–111–115–114
- Liang J, Wu S, You J (1999) The research on variations of onset time of the SCS summer monsoon and its intensity. *J Trop Meteorol* 2:97–105 (in Chinese)
- Liu Y, Huang G, Huang R (2011) Inter-decadal variability of summer rainfall in Eastern China detected by the Lepage test. *Theor Appl Climatol* 106:481–488
- Lorenz EN (1963) Deterministic nonperiodic flow. *J Atmos Sci* 20:130–141
- Lorenz EN (1965) A study of the predictability of a 28-variable atmospheric model. *Tellus* 17:321–333
- Madden RA (1976) Estimates of the natural variability of time-averaged sea-level pressure. *Mon Weather Rev* 104:942–952
- Menon S, Hansen J, Nazarenko L, Luo Y (2002) Climate effects of black carbon aerosols in China and India. *Science* 297:2250–2253
- Nitta T, Hu ZZ (1996) Summer climate variability in China and its association with 500 hPa height and tropical convection. *J Meteorol Soc Jpn* 74:425–445
- Rowell DP (1996) Assessing potential seasonal predictability with an ensemble of multidecadal GCM simulations. *J Clim* 11:109–120
- Rowell DP, Folland CK, Maskell K, Ward MN (2010) Variability of summer rainfall over tropical North Africa (1906–92): observations and modelling. *Q J Roy Meteor Soc* 121:669–704
- Shi H, Zhou T, Wan H, Wang B, Yu R (2008) SMIP2 experiment-based analysis on the simulation and potential predictability of Asian summer monsoon. *Chin J Atmos Sci* 32:36 (in Chinese)
- Shukla J, Gutzler D (1983) Interannual variability and predictability of 500 mb geopotential heights over the Northern Hemisphere. *Mon Weather Rev* 111:1273–1279
- Smith TM, Reynolds RW, Peterson TC, Lawrimore J (2008) Improvements to NOAA's historical merged land–ocean surface temperature analysis (1880–2006). *J Clim* 21:2283–2296
- Song F, Zhou T (2015) The crucial role of internal variability in modulating the decadal variation of the East Asian summer monsoon–ENSO relationship during the twentieth century. *J Clim* 28:7093–7107
- Sui CH, Chung PH, Li T (2007) Interannual and inter-decadal variability of the summertime western North Pacific subtropical high. *Geophys Res Lett* 34:93–104
- Tao SY, Chen LX (1987) A review of recent research on the East Asian summer monsoon in China. In: CP Chang and TN Krishnamurti (Eds) *Monsoon meteorology*, Oxford University Press, England, pp 60–92
- Trenberth KE (1984) Some effects of finite sample size and persistence on meteorological statistics. Part II: potential predictability. *Mon Weather Rev* 112:2369–2379
- Trenberth KE (1985) Potential predictability of geopotential heights over the southern hemisphere. *Mon Weather Rev* 113:54–64
- Wang B, Bao Q, Hoskins B, Wu G, Liu Y (2008a) Tibetan Plateau warming and precipitation changes in East Asia. *Geophys Res Lett* 35(14):63–72
- Wang B, Fan Z (1999) Choice of South Asian summer monsoon indices. *B Am Meteorol Soc* 80:629–638
- Wang B, Wu R, Fu X (2000) Pacific–East Asian teleconnection: how does ENSO affect east Asian climate? *J Clim* 13:1517–1536
- Wang B, Wu Z, Li J, Liu J, Chang CP, Ding Y, Wu G (2008b) How to measure the strength of the East Asian summer monsoon. *J Clim* 21:4449–4463
- Wang B, Yang J, Zhou T, Wang B (2008c) Inter-decadal changes in the major modes of Asian–Australian monsoon variability: strengthening relationship with ENSO since the late 1970s. *J Clim* 21:1771–1789
- Webster PJ, Yang S (1992) Monsoon and ENSO: selectively interactive systems. *Q J Roy Meteor Soc* 118:877–926
- Wu B, Li T, Zhou T (2010a) Relative contributions of the Indian Ocean and local SST anomalies to the maintenance of the western North Pacific anomalous anticyclone during the El Niño decaying summer. *J Clim* 23:2974–2986
- Wu B, Zhang R, Wang B (2009a) On the association between spring Arctic sea ice concentration and Chinese summer rainfall: a further study. *Adv Atmos Sci* 26:666–678
- Wu G, Liu Y, Dong B, Liang X, Duan A, Bao Q, Yu J (2012a) Revisiting Asian monsoon formation and change associated with Tibetan Plateau forcing: I. Formation. *Clim Dynam* 39:1183–1195
- Wu G, Liu Y, Dong B, Liang X, Duan A, Bao Q, Yu J (2012b) Revisiting Asian monsoon formation and change associated with Tibetan Plateau forcing: II. Change. *Clim Dynam* 39:1183–1195
- Wu RG, Wen ZP, Song Y, Li YQ (2010b) An inter-decadal change in Southern China summer rainfall around 1992/93. *J Clim* 23:2389–2403
- Wu Z, Li J, Jiang Z, He J, Zhu X (2012c) Possible effects of the North Atlantic oscillation on the strengthening relationship between the East Asian summer monsoon and ENSO. *Int J Climatol* 32:794–800
- Wu Z, Wang B, Li J, Jin FF (2009b) An empirical seasonal prediction model of the East Asian summer monsoon using ENSO and NAO. *J Geophys Res* 114:85–86
- Wu Z, Yu L (2016) Seasonal prediction of the East Asian summer monsoon with a partial-least square model. *Clim Dynam* 46:3067–3078
- Xie SP, Kosaka Y, Du Y, Hu K, Chowdary JS, Huang G (2016) Indo-western Pacific Ocean capacitor and coherent climate anomalies in post-ENSO summer: a review. *Adv Atmos Sci* 33:411–432
- Xu Q (2001) Abrupt change of the mid-summer climate in central east China by the influence of atmospheric pollution. *Atmos Environ* 35:5029–5040
- Xue F (2001) Interannual to inter-decadal variation of east asian summer monsoon and its association with the global atmospheric circulation and sea surface temperature. *Adv Atmos Sci* 18:567–575. <https://doi.org/10.1007/s00376-001-0045-x>
- Yang J, Liu Q, Xie SP, Liu Z, Wu L (2007) Impact of the Indian Ocean SST basin mode on the Asian summer monsoon. *Geophys Res Lett* 34(2):155–164
- Zhang L, Sielmann F, Fraedrich K, Zhu X, Zhi X (2015) Variability of winter extreme precipitation in Southeast China: contributions of SST anomalies. *Clim Dynam* 45:2557–2570
- Zhang Q, Tao S, Chen L (2003) The interannual variability of East Asian summer monsoon indices and its association with the pattern of general circulation over East Asia. *Acta Meteorol Sin* 61:559–568
- Zhang W, Li H, Stuecker MF, Jin FF, Turner AG (2016) A new understanding of El Niño's impact over East Asia: dominance of the ENSO combination mode. *J Clim* 29:4347–4359
- Zhao Y, Xu X, Zhao T, Xu H, Mao F, Sun H, Wang Y (2016) Extreme precipitation events in East China and associated moisture transport pathways. *Sci China Earth Sci* 59:1854–1872
- Zheng X, Nakamura H, Renwick JA (2000) Potential predictability of seasonal means based on monthly time series of meteorological variables. *J Clim* 13:2591–2604
- Zhou T, Gong D, Li J, Li B (2009) Detecting and understanding the multi-decadal variability of the east Asian summer monsoon—recent progress and state of affairs. *Meteorol Z* 18:455–467
- Zhu Y (2003) Relationships between Pacific decadal oscillation (PDO) and climate variabilities in China. *Acta Meteorol Sin* 61:641–654